Powder Technology 399 (2022) 117151

Contents lists available at ScienceDirect

Powder Technology

journal homepage: www.elsevier.com/locate/powtec

Prediction of the particle size distribution of the aerosol generated by a pressurized metered-dose inhaler

Yamila L. de Charras [a,c,*], M. Verónica Ramírez-Rigo [b,c], Diego E. Bertin [a,c]

[a] Departamento de Ingeniería Química, Universidad Nacional del Sur (UNS), Argentina
[b] Departamento de Biología, Bioquímica y Farmacia, Universidad Nacional del Sur (UNS), Argentina
[c] Planta Piloto de Ingeniería Química – PLAPIQUI (UNS-CONICET), Camino La Carrindanga Km. 7, 8000 Bahía Blanca, Argentina

ARTICLE INFO

Article history:
Received 13 August 2021
Received in revised form 29 December 2021
Accepted 19 January 2022
Available online 25 January 2022

Keywords:
Aerosol technology
Particle size distribution
Respiratory drug delivery
Mathematical model

ABSTRACT

Pressurized metered dose inhalers (pMDIs) are devices widely used for drug delivery in the respiratory tract. In this work, a mathematical model to predict the complete particle size distribution (PSD) of the aerosol generated by a pMDI is developed. The model combines the equations developed by Clark in 1999 that describe the flow within the inhaler, the Linear Instability Sheet Atomization (LISA) model and a method based on the Maximum Entropy Principle (MEP). Mathematically it is found that the PSD can be represented by a lognormal function with geometric standard deviation equal to 1.56. The model does not contain fitting parameters and is validated with experimental information for a formulation containing salbutamol and HFA-134a as drug and propellant, respectively. Simulations are performed to explore how the propellants HFA-134a and HFA-227ea affect the PSD of the aerosol generated by the inhaler.

1. Introduction

Inhalation therapy is fundamental for the treatment of respiratory diseases. In particular, asthma is a chronic inflammatory disorder whose symptoms include wheezing, coughing, shortness of breath and chest tightness [11]. The number of affected patients is increasing exponentially and by 2025 it is estimated that there will be around 400 million people worldwide [20]. Two types of medications to treat asthma are anti-inflammatories and bronchodilators. Anti-inflammatories decrease the inflammation and the mucus production [17]. On the other hand, bronchodilators relax the airway smooth muscle, opening them and making it easier to breathe and expel mucus [5].

Pressurized metered dose inhalers (pMDIs) are widely used devices for drug delivery in the respiratory tract [36]. The pMDI is a small, cost-effective and portable device that consists of an aluminum canister containing a pressurized formulation of the therapeutically active pharmaceutical ingredient (API) dispersed or dissolved in propellants [18,31]. Surfactants, cosolvents, preservatives and flavorings can also be part of the formulation [12]. When the canister (lodged in a plastic actuator) is press down, the valve is opened and an aerosol containing the API is expelled from the pMDI by the expansion of the propellant [26]. The generated aerosol is polydisperse and its particle size distribution (PSD) is a function of the pMDI geometry, physical properties of the formulation and ambient conditions [33]. The PSD measurements are routinely used in product development and quality assurance procedures. Mathematical models can provide information on the PSDs of aerosols generated by pMDIs, allowing to reduce the number of experiments needed to characterize aerosol plumes and, therefore, saving resources.

Clark [6] developed a mathematical model to describe the transient change in mass, temperature, and outlet flow from metering and expansion chambers. The model was capable of predicting the spray nozzle exit conditions as a function of the geometry of the pMDI and the propellant thermodynamic properties. In addition, Clark [6] proposed an empirical correlation to calculate a mean droplet size as a function of the peak pressure developed in the expansion chamber and the vapor quality. Dunbar [8] validated the Clark's correlation with Phase Doppler anemometry (PDA) experimental data. Clark's atomization model is considered the best approach for the prediction of mean particle size generated in a pMDI, although it does not provide the complete particle size distribution.

Smyth et al. [32] analyzed the factors that influence pMDI spray patterns, such as orifice diameter, particle size, and particle size dynamics in the plume. The results indicated that the spray patterns are ellipsoidal and asymmetric, dependent on the inhaler orifice size and may be influenced by the fluid dynamics inside the pMDI. Furthermore, they concluded that the particle size distributions may be related to the evaporation and sedimentation processes of the particles that occur after atomization.

* Corresponding author at: Planta Piloto de Ingeniería Química – PLAPIQUI (UNS-CONICET), Camino La Carrindanga Km. 7, 8000 Bahía Blanca, Argentina.
E-mail address: ydecharras@plapiqui.edu.ar (Y.L. de Charras).

https://doi.org/10.1016/j.powtec.2022.117151
0032-5910/

Kleinstreuer et al. [16] developed and experimentally validated a computational fluid dynamic model (CFD) to simulate the airflow, transport and particle deposition of an aerosol generated by pMDI. They used a model of the human upper airways and analyzed the results in different situations including different propellants (HFA-134a and mixture of CFC-11 and CFC-12) and orifice diameters. The results showed that the smallest particles, responsible for treatment efficacy, are generated by the HFA propellant and smaller valve orifices.

Stein et al. [34] developed a model to predict particle size distributions of the plume generated by pMDI with a drug in suspension. They considered that for inhalers with high drug concentration or micronized particles, a fraction of them may contain multiple drug particles, increasing the particle size distribution emitted. In this model for suspensions, unlike the model for drugs in solution, the number of drug particles contained in the droplet must be determined from the Poisson statistical distribution function and then the size of the particles must be determined by random sampling. This gives a more polydisperse distribution where larger droplets are more likely to contain more than one drug particle. Those droplets that do not contain drug have a final aerodynamic diameter proportional to the initial diameter and the diameter of the drug-containing droplets is given by the mass of the drug particles. Furthermore, they showed that the concentration of drug particles in suspension increases proportionally with the increase of the drug concentration in the formulation and increases according to the third power if the size of the drug decreases. They showed that the percentage of drops containing drug depends on the concentration in the suspension and the initial size, being generally less than 10%.

Oliveira et al. [24] used CFD to characterize and simulate a pMDI spray plume. Using a high-speed camera, they verified that the duration of the spray is 0.1 s and that the spray angle is 17°. In the CFD model, they considered the temperature, velocity, turbulence, particle tracking and propellant evaporation. They showed that the atomization depends on the inhaler pressure, so that the highest proportion of drug is released in the first instants.

Shaik and Versteeg [30], implemented a numerical model to predict the mass flow, pressure, temperature and vapor quality in twin-orifice of pMDI. In this model it is assumed that the propellant flow is in three phases: vapor, saturated liquid and metastable liquid described by the delayed equilibrium model (DEM). This model assumes that evaporation does not occur instantaneously but that a fraction of the propellant remains as a metastable liquid, so there is no thermodynamic equilibrium. Furthermore, it assumes that droplet formation occurs by instantaneous atomization due to the rapid acceleration of the mixture at the spray orifice and the very large pressure drop.

The most used model to predict the spray breakup in atomization systems is the linear instability sheet atomization (LISA) model, proposed by Senecal et al. [29]. Fung et al. [10] combined the LISA spray model with CFD simulations to study the delivery of drugs using pMDIs. They found that the largest droplets tend to move along the central axis and moved with the liquid sheet direction due to inertial effects. On the other hand, small droplets are driven to disperse to peripheral region. Gavtash et al. [13] implemented a CFD model of the development of a pMDI aerosol plume and used the LISA model to predict the spray velocity and the temperature of the plume. They observed that the plume slows down and reaches its final temperature quickly. They also concluded that the particles obtain their final size of 3–5 μm at the nozzle due to propellant evaporation. Later, these same authors [14] compared three two-phase flow models to predict flow conditions in pMDI: the slip equilibrium model (SEM), the homogeneous frozen model (HFM) and the homogeneous equilibrium model (HEM). They found that the HFM velocity prediction best matches the experimental results of Doppler phase anemometry, while the liquid velocity predicted by SEM is well below the plume velocity.

Aiming to have a detailed representation of the aerosol produced by a pMDI, in this work a mathematical model to predict the size of droplets produced by pMDI is developed. Unlike other previously published contributions, this mathematical model is capable of predicting the complete particle size distribution (PSD) without the need for parameter adjustment. Following the guidelines of Gavtash et al. [14], a representative diameter of the aerosol is obtained by combining mass and energy balances within the inhaler developed by Clark with the Linear Instability Sheet Atomization (LISA) model [29]. Then, a method based on the Maximum Entropy Principle (MEP) is proposed to obtain the PSD of the aerosol restricted to the previously calculated representative diameter. The mathematical model is validated with experimental data. As shown in the next section, the developed model does not contain fitting parameters. Simulations are performed to explore how the propellants HFA-134a and HFA-227ea impact the PSD of the aerosol generated by the inhaler.

2. Mathematical model

Fig. 1 shows a simplified schematic representation of a typical pMDI. The pMDI has several components, each of which is important for the correct performance of the entire device [23]. In particular, the actuation system is formed by metering chamber, expansion chamber, metering valve and nozzle orifice (Fig. 2). The effective delivery system consists of two chambers, one for metering and one for expansion, which are connected by a metering valve. The metering valve must deliver the formulation accurately and reproducibly each time the device is actuated [25]. In addition, the metering valve must allow a representative sample of the suspended drug and have an adequate seal due to its high-pressure level [35].

The metering chamber has a measured volume that typically varies between 25 and 100 μL and is connected to the formulation bulk. When the actuator is pressed, the process of the metered discharge of the supercooled liquid formulation begins [8]. The pressure difference between the propellant and atmosphere causes the formulation to release through the valve orifice into the expansion chamber and overheat [27]. The expansion chamber is located between the valve orifice and the nozzle orifice. Its main function is to provide the time necessary for the pressurized propellant to begin to boil and to form a mixture of liquid and vapor as it is released from the device [23]. At the outlet of the inhaler is the nozzle orifice that allows controlling the atomization process of the drug and the formation of the spray. Here the fluid is metastable and as the liquid stream discharges outwards it accelerates. It is in this zone where the high-speed gas flow breaks down into droplets and the primary atomization process occurs [8].

The model of the pMDI is formulated based on the following assumptions:

i. Both the metering and expansion chambers are perfectly mixed and operate adiabatically and at non-steady state conditions [6].
ii. In the metering chamber, equilibrium conditions are maintained [6].
iii. Based on the Homogeneous Frozen Model [9], the steam quality in the nozzle is the same as that of the expansion chamber.
iv. At the pMDI outlet, the liquid forms a thin annular sheet along the walls of the nozzle, surrounding the vapor flow moving in the core [37]. Therefore, the LISA model [29] is valid to predict a representative diameter of the aerosol.
v. The relative velocity between liquid and vapor phases is equal to two-phase flow velocity [19].
vi. The volume PSD of the generated aerosol is lognormally distributed [31,39].

2.1. Metering chamber

When the actuator is pressed, the metering chamber is filled with liquid, at conditions P_{mc0} and T_{mc0}, which are considered equal to those of the canister. Also, T_{mc0} is considered equal to ambient temperature. By pressing the actuator, the liquid-vapor mixture passes from the metering chamber to the expansion chamber.

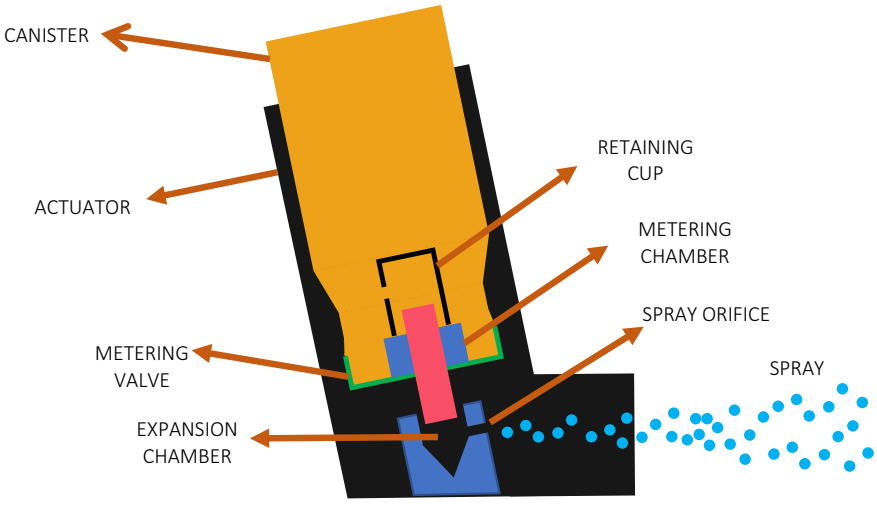

Fig. 1. Schematic representation of a pMDI.

The mass balance for the metering chamber is:

$$\frac{dm_{mc}}{dt} = -\dot{m}_v \tag{1}$$

where m_{mc} is the mass in the metering chamber and $\dot{m}_v$ is the mass flowrate through the valve. Since initially the mixture in the metering chamber is liquid, therefore the initial condition of Eq. (1) is:

$$m_{mc}(0) = \rho_{l,mc} V_{mc} \tag{2}$$

where $\rho_{l,mc}$ is the liquid density and V_{mc} is the metering chamber volume.

$\dot{m}_v$ depends on the pressure difference between metering and expansion chambers:

$$\dot{m}_v = \rho_{mc} C_{Dvalve} A_{valve} \sqrt{\frac{2(P_{mc} - P_{ec})}{\rho_{mc}}} \tag{3}$$

ρ_{mc} is the density of the liquid-vapor mixture in the metering chamber, C_{Dvalve} is the coefficient of the valve and A_{valve} is the area of the valve. P_{mc} and P_{ec} correspond to the pressure in the metering and expansion chamber, respectively. P_{mc} is calculated as the vapor pressure of the liquid-vapor mixture as a function of the chamber temperature:

$$P_{mc} = P^v(T_{mc}) \tag{4}$$

The liquid-vapor mixture density is calculated as:

$$\rho_{mc} = \frac{m_{mc}}{V_{mc}} \tag{5}$$

The temperature of the metering chamber is obtained from an energy balance [6]:

$$T_{mc} = T_{mc0} - \frac{q_{mc} \Delta H_{v,mc}}{q_{mc} cp_{g,mc} + (1 - q_{mc}) cp_{l,mc}} \tag{6}$$

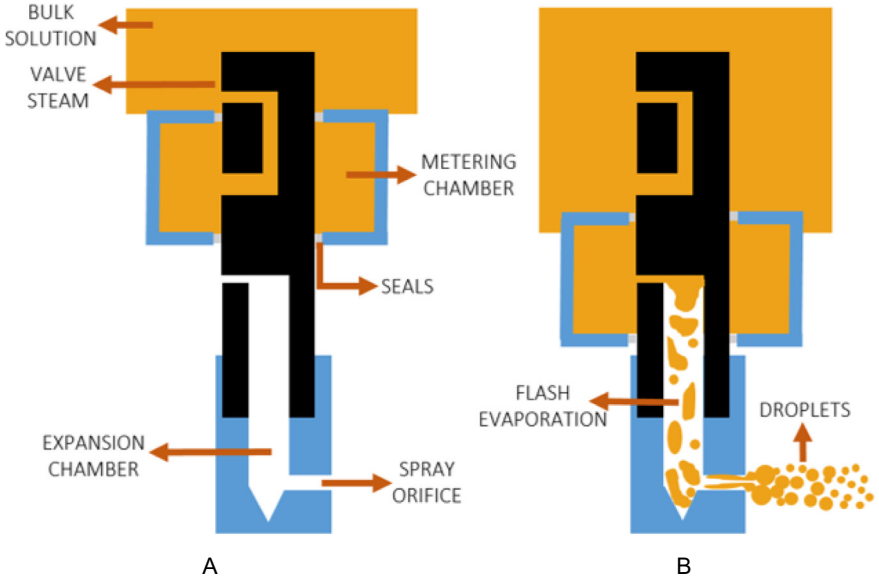

Fig. 2. Schematic of the components of an MDI valve prior to actuation (A) and during actuation (B), adapted from Ivey et al. [15].

$\Delta H_{v,mc}$, $cp_{g,mc}$ and $cp_{l,mc}$ correspond to the vaporization heat and the specific heat of the gas and liquid, respectively, evaluated at metering chamber conditions.

The mass fraction of vapor in the metering chamber is:

$$q_{mc} = \frac{\frac{1}{\rho_{mc}} - \frac{1}{\rho_{l,mc}}}{\frac{1}{\rho_{g,mc}} - \frac{1}{\rho_l}} \tag{7}$$

where $\rho_{g,mc}$ is the density of the vapor in the metering chamber, which is obtained by the ideal gas law:

$$\rho_{g,mc} = \frac{P_{mc} M_{prop}}{R T_{mc}} \tag{8}$$

2.2. Expansion chamber

The mass balance for the expansion chamber is:

$$\frac{dm_{ec}}{dt} = \dot{m}_v - \dot{m}_n \tag{9}$$

where $\dot{m}_n$ is the flowrate through the outlet nozzle. Initially, the expansion chamber is filled with ambient air. The initial air mass (i.e., initial condition of Eq. (9)) is calculated as:

$$m_{ec}(0) = \frac{P_{atm} M_{air}}{R T_{amb}} V_{ec} \tag{10}$$

where M_{air} is the molecular weight of air and V_{ec} is the volume of the expansion chamber. P_{atm} and T_{amb} are the atmospheric pressure and ambient temperature.

According to hypothesis i, it is considered that the initial air leaves the expansion chamber proportionally to its mass percentage within the chamber:

$$\frac{dm_{air}}{dt} = -\frac{m_{air}}{m_{ec}} \dot{m}_n \tag{11}$$

$\dot{m}_n$ is calculated as:

$$\dot{m}_n = \rho_n C_{D\,nozzle} A_{nozzle} v_n \tag{12}$$

ρ_n and v_n correspond to the density and velocity at the nozzle (two-phase flow), respectively, while $C_{Dnozzle}$ and A_{nozzle} are the discharge coefficient and the nozzle area.

The pressure in the expansion chamber is computed by adding the contributions of the vaporized propellant and the air:

$$P_{ec} = P^v(T_{ec}) + \frac{m_{air} R T_{ec}}{M_{air} V_{g,ec}} \tag{13}$$

where $V_{g,ec}$ is the volume of the expansion chamber occupied with gas phase:

$$V_{g,ec} = V_{ec} - \frac{(1-q_{ec}) m_{ec}}{\rho_{l,ec}} \tag{14}$$

being q_{ec} the mass fraction of gas phase in the expansion chamber.

The expansion chamber temperature is obtained from an energy balance:

$$m_{ec} cp_{ec} \frac{dT_{ec}}{dt} = \dot{m}_v \left[q_{mc} cp_{v,(mc,ec)} + (1-q_{mc}) cp_{l,(mc,ec)} \right] \times (T_{mc} - T_{ec}) - \dot{m}_{pv} \Delta H_{v,ec} \tag{15}$$

Where $\dot{m}_{pv}$ is the mass flow rate of propellant being vaporized inside the expansion chamber and $cp_{v,(mc,ec)}$ and $cp_{l,(mc,ec)}$ are the specific heat of the propellant vapor and liquid, respectively, calculated at an average temperature between those of the metering and expansion chambers. $\Delta H_{v,ec}$ is the vaporization heat evaluated at expansion chamber conditions. cp_{ec} is the specific heat of the expansion chamber mixture:

$$cp_{ec} = q'_{ec} cp_{v,ec} + (1-q_{ec}) cp_{l,ec} + (q_{ec} - q'_{ec}) cp_{a,ec} \tag{16}$$

The gas density is calculated from the ideal gas equation:

$$\rho_{g,ec} = \frac{P_{ec}(m_{air} + q'_{ec} m_{ec})}{\left(\frac{m_{air}}{M_{air}} + \frac{q'_{ec} m_{ec}}{M_{prop}}\right) R\, T_{ec}} \tag{17}$$

where q_{ec}' is the mass fraction of propellant vapor (that is, the mass fraction of the gas phase in the expansion chamber without considering the air):

$$q'_{ec} = q_{ec} - \frac{m_{air}}{m_{ec}} \tag{18}$$

The mass fraction of the gas phase (vaporized propellant and air) is:

$$q_{ec} = \frac{\frac{1}{\rho_{ec}} - \frac{1}{\rho_{l,ec}}}{\frac{1}{\rho_{g,ec}} - \frac{1}{\rho_{l,ec}}} \tag{19}$$

where $\rho_{l,ec}$ is the liquid density in the expansion chamber and $\rho_{ec}$is

$$\rho_{ec} = \frac{m_{ec}}{V_{ec}} \tag{20}$$

2.3. pMDI nozzle flow

The pressure at the nozzle depends on whether the mixture reaches the speed of sound:

$$P_n = \begin{cases} P_{atm} & \text{if } P_{atm} > P_{crit} \text{ (subsonic condition)} \\ P_{crit} & \text{if } P_{atm} \le P_{crit} \text{ (sonic condition)} \end{cases} \tag{21}$$

The critical pressure P_{crit} is calculated from the pressure in the expansion chamber P_{ec} and the critical factor r_{crit}:

$$P_{crit} = r_{crit} P_{ec} \tag{22}$$

According to Clark [6], r_{crit} is:

$$r_{crit} = \left[\frac{2(1-q_e)}{\gamma - 1 + 2(1-q_e)} \right]^{\frac{\gamma}{\gamma-1}} \tag{23}$$

where γ is the isentropic expansion factor. For subsonic flow, the velocity at the nozzle is obtained by solving the Bernoulli equation for a two-phase system. If the flow is sonic, the velocity is that of sound for a two-phase system [38]. Then:

$$v_n = \begin{cases} \sqrt{2 \frac{1-q_e}{\rho_l} (P_{ec} - P_{atm}) + \frac{2 q_e P_{ec}^{\frac{1}{\gamma}}}{\rho_{g,ec} \left(1 - \frac{1}{\gamma}\right)} \left({P_{ec}}^{1-\frac{1}{\gamma}} - {P_{atm}}^{1-\frac{1}{\gamma}} \right)} & \text{if } P_{atm} > P_{crit} \\ \sqrt{\frac{\gamma q_e P_{ec}}{\rho_{g,ec}(1-q_e)} {r_{crit}}^{1-\frac{1}{\gamma}}} & \text{if } P_{atm} \le P_{crit} \end{cases} \tag{24}$$

The temperature and gas density at the nozzle are obtained considering adiabatic expansion:

$$T_n = T_{ec}\left(\frac{P_n}{P_{ec}}\right)^{\frac{\gamma-1}{\gamma}} \tag{25}$$

$$\rho_{g,n} = \rho_{g,ec}\left(\frac{P_n}{P_{ec}}\right)^{\frac{1}{\gamma}} \tag{26}$$

The two-phase flow density at the nozzle is calculated as:

$$\rho_n = \frac{1}{\frac{q_e}{\rho_{g,n}} + \frac{1-q_e}{\rho_l}} \tag{27}$$

According to the hypothesis iii, it is considered that the quality of vapor q_e in the nozzle is the same as that of the expansion chamber.

Senecal et al. [29] describes the aerosol mass flowrate as:

$$\dot{m}_{SO} = 2\pi\rho_{l,SO} v_n h_b (D - 2h_b) \tag{28}$$

D is the diameter of the nozzle, $\rho_{l,SO}$ is the liquid density in the spray orifice and h_b is the thickness of the annular liquid film at the breakup point. Based on hypothesis iii, Gavtash et al. [14] found that h_b can be calculated as:

$$h_b = \frac{D}{2}(1 - \sqrt{\alpha}) \tag{29}$$

where α is the volumetric fraction of vapor in the mixture:

$$\alpha = \frac{1}{1 + \frac{1-q_{ec}}{q_{ec}}\frac{\rho_{g,n}}{\rho_{l,n}}} \tag{30}$$

2.4. Representative diameter of the aerosol

The LISA (Linearized Instability Sheet Atomization) model was developed by Senecal et al. [29] to simulate the primary atomization process of the emerging liquid film from a high-pressure swirl nozzle. The model is based on a linear stability analysis, according to which instabilities that occur at the gas-liquid interface produce ligaments, which broke up into droplets. Senecal et al. [29] considered a two-dimensional liquid sheet, where the instability is mainly due to aerodynamic interactions between the liquid and the gas. Unlike cylindrical liquid jets, surface tension forces tend to stabilize a planar liquid sheet [3].

According to Senecal et al. [29], the droplet formation can occur in two different regimes according to: (a) short waves that are dominated by viscous and surface tension effects and (b) long waves, which are governed by surface tension and inertial effects:

$$\begin{cases} We_{g,h_b} < \frac{27}{16}: & long\ waves \\ We_{g,h_b} \geq \frac{27}{16}: & short\ waves \end{cases} \tag{31}$$

We_{g,h_b} is the gas Weber number:

$$We_{g,h_b} = \frac{\rho_{g.n} v_n^2 h_b}{2\sigma_p} \tag{32}$$

where σ_p is the surface tension.

The diameter of ligaments is calculated as:

$$d_L = \begin{cases} \sqrt{\frac{4h_b}{k_{max}}}: & long\ waves \\ \frac{2\pi C_L}{k_{max}}: & short\ waves \end{cases} \tag{33}$$

where by default it is considered $C_L = 0.5$. k_{max} is the wave number that maximizes the wave growth rate. For long waves, Senecal et al. [29] suggests calculating k_{max} as:

$$k_{max} = \frac{\rho_{g,n} v_n^2}{2\sigma} \tag{34}$$

On the other hand, for short waves, k_{max} is the value of k that maximizes the following expression of ω [2,29]:

$$\omega = -2\nu_{l,n}k^2 + \sqrt{4\nu_{l,n}^2 k^4 + Q v_n^2 k^2 - \frac{\sigma_p k^3}{\rho_{l,n}}} \tag{35}$$

where:

$$\nu_{l,n} = \frac{\mu_{l,n}}{\rho_{l,n}} \tag{36}$$

$$Q = \frac{\rho_{g,n}}{\rho_{l,n}} \tag{37}$$

$\mu_{l,\,n}$ is the viscosity of the liquid leaving the nozzle.

If Eq. (35) is derived with respect to k and the resulting expression is set equal to zero, the following equation to calculate k_{max} is obtained:

$$4\nu_{l,n}k_{max} - \frac{16\nu_{l,n}^2 k_{max}^3 + 2Q v_n^2 k_{max} - \frac{3\sigma k_{max}^2}{\rho_{l,n}}}{2\sqrt{4\nu_{l,n}^2 k_{max}^4 + Q v_n^2 k_{max}^2 - \frac{\sigma k_{max}^3}{\rho_{l,n}}}} = 0 \tag{38}$$

For both regimes, a particle is formed when the amplitude of the unstable waves is equal to the radius of the ligament. According to Senecal et al. [29], the most probable droplet diameter is:

$$d_{Dso} = 1.88\,(1 + 3Oh_L)^{\frac{1}{6}}\, d_L \tag{39}$$

where Oh_L is the Ohnesorge number for the ligaments:

$$Oh_L = \frac{\mu_{l,n}}{\sqrt{\rho_{l,n}\sigma_p d_L}} \tag{40}$$

Gavtash et al. [14] consider that droplets flash evaporation occurs very quickly as soon as the spray leaves the nozzle. The propellant mass fraction lost by evaporation can be obtained from an energy balance:

$$\Delta x_{no} = \frac{cp_{l,(n,amb)}(T_n - T_{amb})}{\Delta H_{v,(n,amb)}} \tag{41}$$

$cp_{l,(n,amb)}$ and $\Delta H_{v,(n,amb)}$ are evaluated at an average temperature between T_n and T_{amb}. Then, from a mass balance for an aerosol particle, the particle diameter after flash evaporation is [14]:

$$d_{Dno} = d_{Dso}\left[\frac{\rho_{l,so}}{\rho_{l,(sat,amb)}}(1 - \Delta x_{no})\right]^{1/3} \tag{42}$$

$\rho_{l,(sat,amb)}$ is the liquid density evaluated at an average temperature between that corresponding to saturation state at ambient pressure and T_{amb}.

2.5. Particle size distribution

In other areas of application, the method of the Maximization of Entropy Principle (MEP) has been widely used to predict the size of the droplets formed in atomization processes. The MEP method starts from considering that the droplets formation is a random process [7].

Besides, during the droplet formation occurs a transformation from one equilibrium state in the outlet of the injector to another downstream where droplets are formed from ligaments [22]. Then, according to thermodynamics laws, this state change involves an entropy increase until it reaches a maximum value. Therefore, the distribution of droplets with respect to internal coordinates (e.g., diameter, velocity) can be calculated by maximizing the entropy of the distribution (i.e., Shannon entropy), as long as a series of constraints are satisfied. According to the probability concept, one of these restrictions is that the total summation of number fractions should be equal to unity. The remaining restrictions are established from the conservation equation [21].

According to hypothesis vi, the volume droplet size distribution follows a lognormal function:

$$f_v(d) = \frac{1}{\ln\sigma\sqrt{2\pi}\,d}\exp\left[-\frac{1}{2}\left(\frac{\ln d - \ln d_{v50}}{\ln\sigma_g}\right)^2\right] \tag{43}$$

d_{v50} is the geometric mean diameter of the function and σ_g is the geometric standard deviation which is a measure of the width of the distribution. Eq. (43) is a density function that indicates the probability of finding a certain volume of liquid with drops with diameter d.

Since the maximization of entropy must be applied to a distribution expressed in number of droplets instead of volume [7], it is necessary to convert Eq. (43) to a density function in number. According to Allen [1], the equivalence between the number and volume density function ($f_n(d)$ and $f_v(d)$, respectively) is:

$$f_n(d) = \left(\frac{d_{NV}}{d}\right)^3 f_v(d) \tag{44}$$

where d_{NV} is the number-volume mean diameter of the distribution.

Replacing Eqs. (43) in (44):

$$f_n(d) = \frac{{d_{NV}}^3}{\ln\sigma_g\sqrt{2\pi}\,d^4}\exp\left[-\frac{1}{2}\left(\frac{\ln d - \ln d_{v50}}{\ln\sigma_g}\right)^2\right] \tag{45}$$

Considering the properties of the lognormal function, the d_{NV} can be written as [1]:

$${d_{NV}}^3 = {d_{v50}}^3 e^{-\frac{9}{2}\left(\ln\sigma_g\right)^2} \tag{46}$$

Therefore, Eq. (45) can be rewritten as:

$$f_n(d) = \frac{{d_{v50}}^3 e^{-\frac{9}{2}\left(\ln\sigma_g\right)^2}}{\ln\sigma_g\sqrt{2\pi}\,d^4}\exp\left[-\frac{1}{2}\left(\frac{\ln d - \ln d_{v50}}{\ln\sigma_g}\right)^2\right] \tag{47}$$

Gavtash et al. [14] found that the d_{Dno} predicted by the LISA model is between the d_{SV} (surface-volume mean or Sauter diameter) and the d_{NL} (number-length mean diameter). In this work, it is assumed that d_{Dno} is equal to d_{SV}. Then, the following relationship is considered [1]:

$$d_{Dno} = d_{SV} = d_{v50}e^{-\frac{1}{2}\left(\ln\sigma_g\right)^2} \tag{48}$$

Combining Eqs. 47 and 48 is obtained:

$$f_n(d) = \frac{{d_{Dno}}^3 e^{-3\left(\ln\sigma_g\right)^2}}{\ln\sigma_g\sqrt{2\pi}\,d^4}\exp\left[-\frac{1}{2}\left(\frac{\ln d - \ln d_{Dno} - \frac{1}{2}\left(\ln\sigma_g\right)^2}{\ln\sigma_g}\right)^2\right] \tag{49}$$

In Eq. (49), due to d_{Dno} is determined from Eq. (42), the only free parameter that remains to be determined is σ_g. To obtain σ_g, the MEP method is applied, which implies maximizing the Shannon entropy [22,28]:

$$S = -\int_0^\infty f_n(d)\ln f_n(d)\,dd \tag{50}$$

Replacing the Eq. (49) in (50) and solving the integral, it is obtained:

$$S = \ln\left\{\sqrt{2\pi}\ln\sigma_g\right\} + \ln d_{Dno} - \frac{5}{2}\left(\ln\sigma_g\right)^2 + \frac{1}{2} \tag{51}$$

The value of σ_g that maximizes S is obtained by deriving the Eq. (51) with respect to σ_g and setting the resulting expression equal to 0. The solution obtained is:

$$\left(\ln\sigma_g\right)^2 = \frac{1}{5} \tag{52}$$

Therefore, it is concluded that, if the volume droplet size distribution is represented by a lognormal function with geometric standard deviation equal to $\sigma_g \approx 1.56$. Furthermore, the volume droplet size distribution expressed as a function of the parameters d_{Dno} and σ_g is:

$$f_v(d) = \frac{1}{\ln\sigma_g\sqrt{2\pi}\,d}\exp\left[-\frac{1}{2}\left(\frac{\ln d - \ln d_{Dno} - \frac{1}{2}\left(\ln\sigma_g\right)^2}{\ln\sigma_g}\right)^2\right] \tag{53}$$

In the appendix it is shown that, if Eqs. (48)–(53) are developed assuming that the diameter d_{Dno} is equal to d_{NL} instead of d_{SV}, a standard deviation equal to 2.72 is obtained. This standard deviation produces a very sparse droplet size distribution that does not make physical sense, so it is not a reasonable hypothesis for applying the entropy method.

3. Particle size measurement

Salbutamol pMDI (Ventolin, GlaxoSmithKline, UK) was used as the reference product, since it is one of the most widely used drugs to treat asthma in children and adults. The propellant contained in the selected dosage form was HFA-134a. The PSD of the aerosol emitted by pMDI was determined by laser diffraction (LD) using a Mastersizer S (Malvern Panalytical, UK). This technique uses Mie's light scattering theory assuming a volume-equivalent sphere model (See Fig. 3). The pMDI actuator was positioned at 8 cm from the detector lens. Before the test, pMDI was shaken for 5 s by hand and fired to discard at least the first 3 spray. Then, it was shaken again and the actuation of the spray to be measured was carried out. All measurements were made at room temperature (24 °C) and at relative humidity close to 60%. Representative particle size distributions and volume diameters were collected using a LD software. PSD was measured in triplicate after one actuation and the results were averaged.

The experimental results were analyzed by analysis of variance (ANOVA) to determine the importance of the differences in the size distributions. Differences were considered significant if $p < 0.05$ with 95% confidence intervals.

4. Results

In Fig. 4, the d_{Dno} predicted by the mathematical model for the HFA-134a propellant is presented. For the calculation, the properties of HFA-134a that were assumed independent of temperature are listed in Table 1. Besides, Table 2 summarizes the correlations of thermodynamic properties as a function of temperature, which were obtained from data reported in the NIST database. The experimental values of d_{SV} and d_{NL} are also shown in Fig. 4. In line with the results of Gavtash et al. [14], the d_{Dno} varies most of the time in the range between d_{SV} and d_{NL}, suggesting that the mean droplet size is calculated correctly., the droplet diameter increases according to Eqs. (33), (39) and (42).

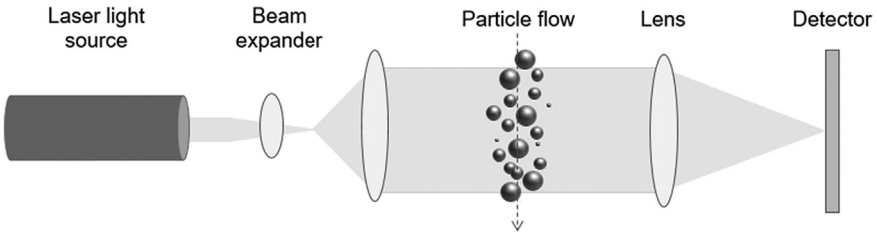

Fig. 3. Schematic diagram of laser diffraction system.

The temporal trend of d_{Dno}indicates that this diameter rapidly rises to approximately 0.02 s and then gradually decreases down to 0.06 s and then increases rapidly. As explained by Gavtash et al. [14], the temporal behavior of d_{Dno} is related to the filling and emptying of the expansion chamber. After 0.06 s, the d_{Dno} increases rapidly, resulting in a non-physical overestimation from 0.1 s. However, according to Fig. 5, for 0.1 s 97% of the aerosol has been emitted. This non-physical behavior occurs because, when the expansion chamber is close to emptying, the flow velocity at the outlet of the orifice decreases, which in turn reduces the value of k_{max} (Eqs. (34) and (38)). Consequently, the droplet diameter increases according to Eqs. (33), (39) and (42).

For a better comparison with the experimental mean diameters d_{SV} and d_{NL}, in Fig. 4 a time averaged d_{Dno} is shown. It is observed that the averaged d_{Dno} evolves up to 2.78 μm. Furthermore, starting at 0.03 s, the time-averaged mean diameter varies by less than ±4% around the final value.

In Fig. 6, the predicted PSD for a pMDI containing HFA-134a propellant is compared with the experimental PSD of the marketed salbutamol pMDI. The experimental particle size distribution corresponds to the average of the three measurements made. Error bars were added to show the variation of the repetitions. It is observed that the three measurements were similar. In addition, the results of the samples indicate that $d_{v50} = 3.58 \pm 0.03$ μm. The predicted PSD is calculated using the time-averaged d_{Dno} value. Without using any fitting parameter, a good agreement between the experimental and simulated values is found. It is likely that the overestimation in the tail of fine particles is due to the fact that the measurement point is located relatively far from the spray orifice. Since it takes time for the droplets to reach the measurement point, small droplets have more time to disperse and may disappear if all the propellant evaporates.

In Fig. 7, the predicted PSD for the HFA-134a propellant is compared with that for the HFA-227ea propellant. Tables 1 and 2 summarize the physical properties used for each propellant. According to Fig. 7, the PSD for HFA-227ea is located towards larger diameters than those for HFA-134a propellant. This result is consistent with those obtained by Brambilla et al. [4] and Gavtash et al. [14]. For HFA-227ea, the time-averaged d_{Dno} is equal to 3.09, i.e., 10.3% greater than time-averaged d_{Dno} for HFA- 134a. Fig. 7 also indicates that the PSD for HFA-134a is narrower compared to HFA-227ea. This is due to the fact that, for the same geometric standard deviation, a lognormal function is narrower the smaller its geometric mean diameter (see Eqs. (43) and (48)).

Fig. 8 shows the temporal variation of the d_{v10}, d_{v50} and d_{v90} for propellants HFA-134a and HFA-227ea, which are obtained from the cumulative size distributions. For both propellants, the simulation time coincides with 97% of the fraction emitted from the aerosol. As expected, the trends for the d_{v10}, d_{v50} and d_{v90} is similar to that of d_{Dno} (see Fig. 4 for HFA-134a). According to Fig. 8, the PSD for HFA-134a becomes wider until it reaches a time of 0.03 s. Then the PSD becomes narrower down to 0.06 s. From this time the PSD becomes wider for HFA-134a. The trends are similar for HFA-227ea, although occurring for longer times.

In Fig. 9, fraction of particles in the respirable size range 0.5–5 μm predicted for the propellants HFA-134a and HFA-227ea is shown. It should be clarified that the respirable range should be obtained with the aerodynamic diameter and not with the geometric one, however the analysis performed is valid for a unit particle density. For HFA-134a, the fraction of respirable particles is greater than 75% until reaching a time of approximately 0.087 s (95% of the total fraction emitted according to Fig. 5). However, for HFA-227ea, the fraction of respirable particles is reduced to a minimum of 60% at 0.03 s. This result indicates that the aerosol generated with the HFA-134a propellant has a higher fraction of respirable particles compared to the HFA-227ea propellant. As mentioned above, HFA-134a propellant is almost totally emitted (97%, see Fig. 5) in 0.1 s. Therefore, the respirable particles fraction tends to zero for that time. The same behavior is observed for the HFA-227ea propellant, which is almost totally emitted in 0.13 s. Around the total emission time, the fraction of respirable particles decreases rapidly. This is due to the non-physical overtimation observed in Fig. 4 (for HFA-134a propellant).

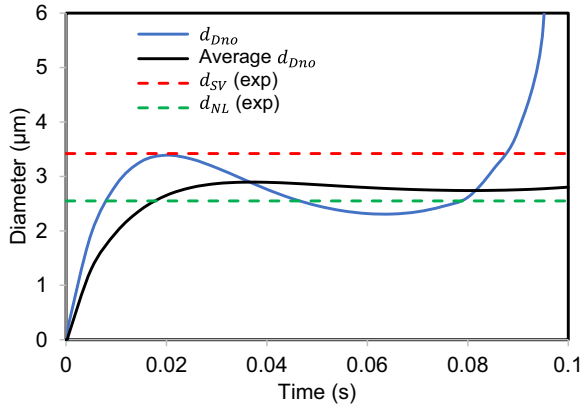

Fig. 4. Comparison of the predicted d_{Dno} with experimental d_{SV} and d_{NL}.

5. Conclusions

A mathematical model to predict the particle size distribution generated in a pMDI has been derived mathematically. The mathematical model has no fit parameters. The mean diameter d_{Dno}, predicted by the LISA model and used by Gavtash et al. [14] was assumed equal to the Sauter diameter of the PSD. From the Maximization of Entropy Principle (MEP), it was found that the PSD is adequately represented by a

Table 1
Propellants properties at 298 K.

Property	HFA-134a	HFA-227ea
Chemical formula	CH_2FCF_3	C_3HF_7
MW (kg/molg)	102	170
Surface tension (N/m)	8.10E-3	7.10E-3
Viscosity (Pa.s)	1.95E-4	2.40E-4
Liquid specific heat capacity (J/kg K)	1424.4	1388.2
Adiabatic coefficient	1.23	1.13

Table 2
Correlations of thermodynamic properties as a function of temperature (NIST).

Property	HFA-134a	HFA-227*ea*
cp_g	$0.0255T^2 - 9.2076T + 1513.7$	$0.0091T^2 - 1.6914T + 599.6$
ρ_l	$-0.0068T^2 + 0.3898T + 1697.6$	$-0.0076T^2 + 0.4710T + 1923.6$
ΔH_v	$-0.2890T^2 + 479.30T + 238407$	$-1.2513T^2 + 206.22T + 161136$
$\log P^v$	$10.346 \ln(T) - 45.494$	$10.672 \ln(T) - 47.728$

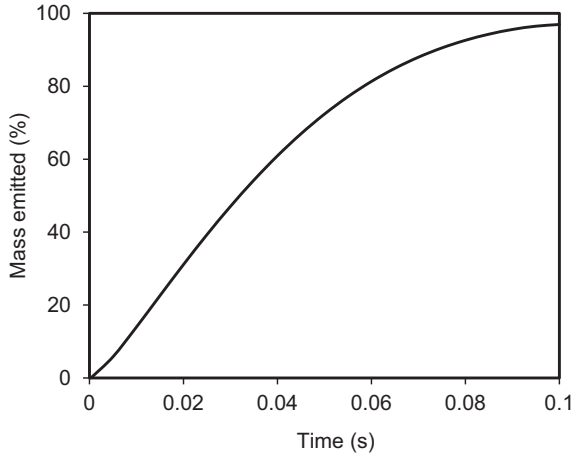

Fig. 5. Mass fraction emitted by the pMDI for the propellant HFA-134a.

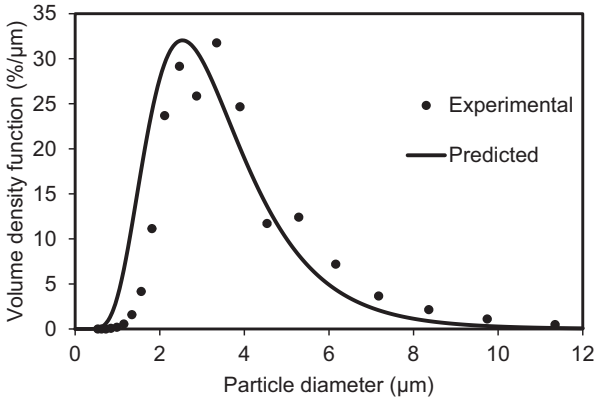

Fig. 6. Comparison of the predicted and experimental PSDs.

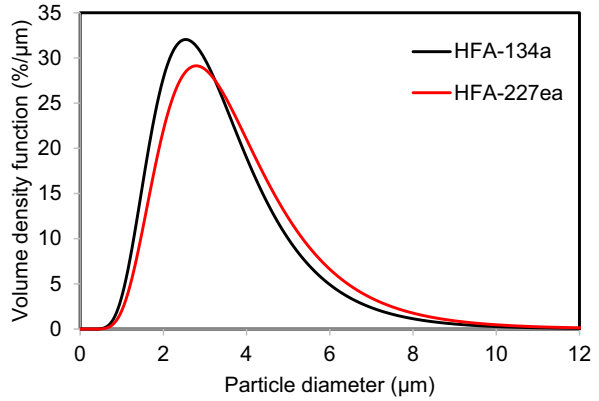

Fig. 7. Comparison of the predicted PSDs for the propellants HFA-134a and HFA- 227ea.

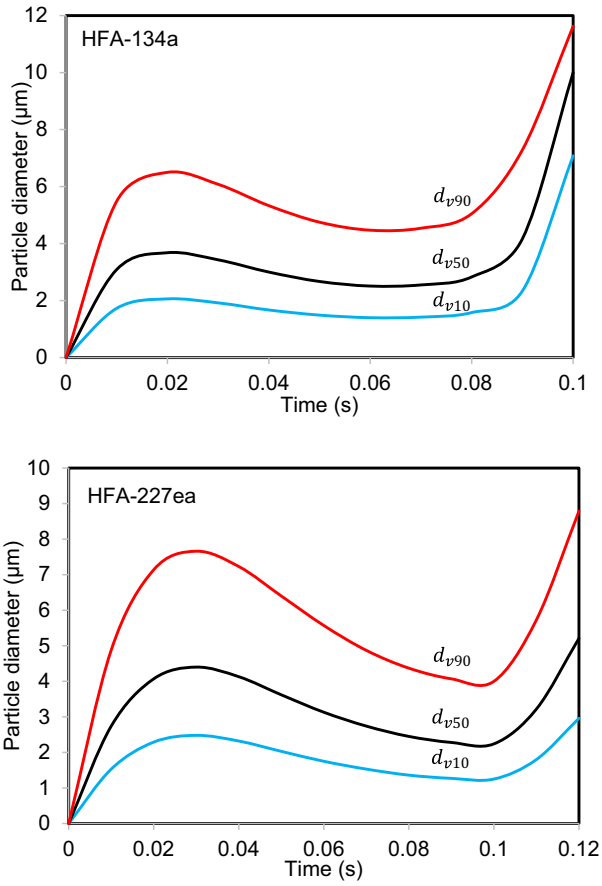

Fig. 8. d_{v10}, d_{v50} and d_{v90} predicted for the propellants HFA-134a and HFA- 227ea.

lognormal function with geometric standard deviation equal to 1.56. The PSD predicted by the model agrees with experimental data.

Due to the mathematical model depends on the physical properties of the propellant used, the calculated PSD varies as a function of the propellant. The analysis of the fraction of respirable particles demonstrated that the aerosol generated by the propellant HFA-134a has a higher fraction of particles in the range 0.5–5 µm in a longer time compared to the propellant HFA-227ea. Although the model predicts DSD at a distance close to the pMDI orifice, this result indicates that the HFA-134 produces more particles in the respirable size than HFA-227ea.

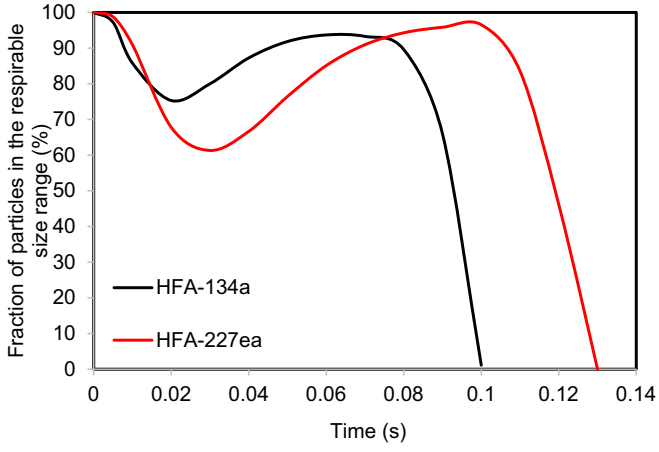

Fig. 9. Fraction of particles in the respirable size range 0.5–5 µm predicted for the propellants HFA-134a and HFA-227ea.

In this contribution, the mathematical model was used with pure propellants. Further work is needed to compare model predictions with DSD experimental data corresponding to other formulations (pure propellants and propellant-excipient mixtures). Special attention deserves the requirement for green propellants, i.e., propellants with lower global warming potentials. To contribute to this transition towards less dangerous propellants for the environment, the developed mathematical model can be used to analyze how the thermophysical properties of new formulations impact the aerosol generation. This pending study deserves further research.

Nomenclature

A_{nozzle}	Nozzle area [m^2].
A_{valve}	Area of the valve [m^2].
C_L	Ligament's constant [−].
$C_{Dnozzle}$	Discharge coefficient [−].
C_{Dvalve}	Coefficient of the valve [−].
ΔH_v	Vaporization heat [J/kg].
h_b	Thickness of the annular liquid film at the breakup point [m].
cp	Specific heat [J/kg K].
cp_g	Specific heat of the gas [J/kg K].
cp_l	Specific heat of the propellant liquid [J/kg K].
d	Droplet/particle diameter [m].
d_{Dno}	Particle diameter after flash evaporation [m].
d_{Dso}	Most probable droplet diameter [m].
d_L	Diameter of ligaments [m].
d_{NL}	Number-length mean diameter of the PSD [m].
d_{NV}	Number-volume mean diameter of the PSD [m]
d_{SV}	Surface-volume mean diameter of the PSD [m]
d_{v50}	Geometric mean diameter of the PSD [m].
D	Diameter of the nozzle [m].
$f_n(d)$	Number droplet size distribution [%/μm].
$f_v(d)$	Volume droplet size distribution [%/μm].
k	Wave number [1/m].
k_{max}	Wave number that maximizes the wave growth rate [1/m]
m	Mass [kg].
$\dot{m}_{SO}$	Aerosol mass flow rate [kg/s].
$\dot{m}_n$	Mass flowrate through the outlet nozzle [kg/s].
$\dot{m}_{pv}$	Mass flow rate of propellant being vaporized inside the expansion chamber [kg/s].
$\dot{m}_v$	Mass flowrate through the valve [kg/s].
M_{air}	Molecular weight of air [kg/mol].
M_{prop}	Propellant molecular weight [kg/mol].
Oh_L	Ohnesorge number for the ligaments [−].
P	Pressure [Pa].
P_{crit}	Critical pressure [Pa].
P^v	Vapor pressure [Pa].
q	Mass fraction of gas phase [−].
q'	Mass fraction of propellant vapor [−].
Q	Ratio between $\rho_{g,\,n}$ and $\rho_{l,\,n}$ [−].
r_{crit}	Critical factor for sonic condition [−].
R	Ideal gas constant [J/mol K].
t	Time [s].
T	Temperature [K].
v	Velocity of two-phase flow [m/s].
V	Volume [m^3].
V_g	Volume occupied with gas phase [m^3].
We_{g,h_b}	Gas Weber number [−].

Greek symbols

α	Volumetric fraction of vapor in the mixture [−]
γ	Isentropic expansion factor [−].
Δx_{no}	Propellant mass fraction lost by evaporation [−]
$\mu_{l,n}$	Viscosity of the liquid leaving the nozzle [kg/m s]
$\nu_{l,n}$	Ratio between $\mu_{l,n}$ and $\rho_{l,n}$ [m^2/s].
ρ	Mixture density [kg/m^3].
ρ_g	Gas density [kg/m^3].
ρ_l	Liquid density [kg/m^3].
$\rho_{l,\,SO}$	Liquid density in the spray orifice [kg/m^3].
ρ_n	Density of two-phase flow at the nozzle [kg/m^3]
σ_g	Geometric standard deviation [−]
σ_p	Surface tension [N/m].

Subscripts

air	Air in the expansion chamber.
amb	Ambient conditions.
ec	Expansion chamber.
mc	Metering chamber.
n	Nozzle.
(n,amb)	Average temperature between T_n and T_{amb}.
(sat,amb)	Average temperature between that corresponding to saturation state at ambient pressure and T_{amb}.

CRediT authorship contribution statement

Yamila L. de Charras: Conceptualization, Methodology, Investigation, Writing – review & editing. **M. Verónica Ramírez-Rigo:** Conceptualization, Writing – review & editing. **Diego E. Bertin:** Conceptualization, Writing – review & editing.

Declaration of Competing Interest

The authors declare that they have no known competing financial interests or personal relationships that could have appeared to influence the work reported in this paper.

Acknowledgment

This work was funded by the Consejo Nacional de Investigaciones Científicas y Técnicas (CONICET, PIP 11220150100704CO), the Agencia Nacional de Promoción Científica y Tecnológica (ANPCyT, PICT-2016-0976; PICT-2018-00735), the Secretaría de Políticas Universitarias (VT42-UNS11688) and the Universidad Nacional del Sur (UNS, PGI 24/B252) from Argentina. d.C.Y.L. thanks ANPCyT for her doctoral fellowship. The authors thank F. Cabrera (PLAPIQUI) for her technical assistance.

Appendix A. Appendix

If it is assumed que d_{Dno} is equal to d_{NL}, the following relationship is satisfied [1]:

$$d_{Dno} = d_{NL} = d_{v50} e^{-\frac{5}{2}(\ln\sigma)^2} \tag{A1}$$

Combining Eqs. (47) and (A1) gives:

$$f_n(d) = \frac{{d_{Dno}}^3 e^{-3(\ln\sigma)^2}}{\ln\sigma\sqrt{2\pi}\,d^4} \exp\left[-\frac{1}{2}\left(\frac{\ln d - \ln d_{Dno} - \frac{5}{2}(\ln\sigma)^2}{\ln\sigma}\right)^2\right] \tag{A2}$$

By replacing the Eq. (A2) in 50, it is obtained:

$$S = \ln\left\{\sqrt{2\pi}\ln\sigma\right\} + \ln d_{Dno} - \frac{1}{2}(\ln\sigma)^2 + \frac{1}{2} \tag{A3}$$

The entropy S is maximized by deriving Eq. (A3) with respect to σ and setting the resulting expression equal to 0. The solution obtained is:

$$(\ln\sigma)^2 = 1 \tag{A4}$$

Therefore:

$$\sigma = e \approx 2.72 \quad \text{(A5)}$$

Consequently, if the volume particle size distribution is represented by a lognormal function whose d_{v10} is equal to the d_{Dno} predicted by the LISA model, then the geometric standard deviation of the distribution is $\sigma \approx 2.72$. As mentioned in the paper, this geometric standard deviation is considerably large and generates a very wide PSD. For this reason, it does not seem reasonable to assume that d_{Dno} is equal to the mean diameter d_{NL}.

References

[1] T. Allen, Powder Sampling and Particle Size Determination, Elsevier, 2003.
[2] ANSYS-Fluent Theory Guide. , ANSYS INC., 2011
[3] N. Ashgriz (Ed.), Handbook of Atomization and Sprays: Theory and Applications, Springer Science & Business Media, 2011.
[4] G. Brambilla, D. Ganderton, R. Garzia, D. Lewis, B. Meakin, P. Ventura, Modulation of aerosol clouds produced by pressurised inhalation aerosols, Int. J. Pharm. 186 (1) (1999) 53–61.
[5] M. Cazzola, A. Segreti, M.G. Matera, Novel bronchodilators in asthma, Curr. Opin. Pulm. Med. 16 (1) (2010) 6–12.
[6] A.R. Clark, Metered Atomisation for Respiratory Drug Delivery, Doctoral dissertation Loughborough University, 1991.
[7] C. Dumouchel, The maximum entropy formalism and the prediction of liquid spray drop-size distribution, Entropy 11 (4) (2009) 713–747.
[8] C.A. Dunbar, A.P. Watkins, J.F. Miller, An experimental investigation of the spray issued from a pMDI using laser diagnostic techniques, J. Aeros. Med. 10 (4) (1997) 351–368.
[9] G.E. Fletcher, Factors Affecting the Atomization of Saturated Liquids, (Doctoral dissertation Loughborough University, 1975.
[10] M.C. Fung, K. Inthavong, W. Yang, J. Tu, CFD modeling of spray atomization for a nasal spray device, Aerosol Sci. Technol. 46 (11) (2012) 1219–1226.
[11] A. Gater, L. Nelsen, S. Fleming, J.J. Lundy, N. Bonner, R. Hall, J. Haughney, Assessing asthma symptoms in adolescents and adults: qualitative research supporting development of the asthma daily symptom diary, Value Health 19 (4) (2016) 440–450.
[12] B. Gavtash, H.K. Versteeg, G. Hargrave, D. Lewis, T. Church, G. Brambilla, ... F. Mason, CFD simulation of pMDI aerosols in confined geometry of USP-IP using predictive spray source, J. Aerosol. Med. Pulm. Drug Deliv 29 (2015).
[13] B. Gavtash, H. Versteeg, G. Hargrave, B. Myatt, D. Lewis, T. Church, G. Brambilla, Multi-Physics Theoretical Approach to Predict pMDI Spray Characteristics, 2016.
[14] B. Gavtash, H.K. Versteeg, G. Hargrave, B. Myatt, D. Lewis, T. Church, G. Brambilla, Transient aerodynamic atomization model to predict aerosol droplet size of pressurized metered dose inhalers (pMDI), Aerosol Sci. Technol. 51 (8) (2017) 998–1008.
[15] J.W. Ivey, D. Lewis, T. Church, W.H. Finlay, R. Vehring, A correlation equation for the mass median aerodynamic diameter of the aerosol emitted by solution metered dose inhalers, Int. J. Pharm. 465 (1–2) (2014) 18–24.
[16] C. Kleinstreuer, H. Shi, Z. Zhang, Computational analyses of a pressurized metered dose inhaler and a new drug–aerosol targeting methodology, J. Aeros. Med. 20 (3) (2007) 294–309.
[17] M. Kupczyk, B. Dahlén, S. Dahlén, Which anti-inflammatory drug should we use in asthma? Pol. Arch. Med. Wewn. 121 (12) (2011) 455–459.
[18] F. Lavorini, The challenge of delivering therapeutic aerosols to asthma patients, International Scholarly Research Notices, 2013, 2013.
[19] A.H. Lefebvre, Atomization and Sprays, Hemisphere Pub, Corp., New York, 1989 1989.
[20] M.C. Maciag, W. Phipatanakul, Prevention of asthma: targets for intervention, Chest 158 (3) (2020) 913–922.
[21] E. Movahednejad, F. Ommi, Development of maximum entropy method for prediction of droplet-size distribution in primary breakup region of spray, Int. J. Chem. Mol. Eng. 5 (11) (2011) 1012–1018.
[22] E. Movahednejad, F. Ommi, S.M. Hosseinalipour, Prediction of droplet size and velocity distribution in droplet formation region of liquid spray, Entropy 12 (6) (2010) 1484–1498.
[23] S.P. Newman, Principles of metered-dose inhaler design, Respir. Care 50 (9) (2005) 1177–1190.
[24] R.F. Oliveira, A.C. Ferreira, S.F. Teixeira, J.C. Teixeira, H.C. Marques, pMDI spray plume analysis: A CFD study, Proceedings of the World Congress on Engineering, (vol. 3, 2013.
[25] U.S. Pharmacopeia, USP, 2008 31.
[26] N. Roche, P.R. Dekhuijzen, The evolution of pressurized metered-dose inhalers from early to modern devices, J. Aerosol Med. Pulm. Drug Deliv. 29 (4) (2016) 311–327.
[27] R.K. Schultz, Drug delivery characteristics of metered-dose inhalers, J. Allergy Clin. Immunol. 96 (2) (1995) 284–287.
[28] R.W. Sellens, T.A. Brzustowski, A simplified prediction of droplet velocity distributions in a spray, Combust. Flame 65 (3) (1986) 273–279.
[29] P.K. Senecal, D.P. Schmidt, I. Nouar, C.J. Rutland, R.D. Reitz, M.L. Corradini, Modeling high-speed viscous liquid sheet atomization, Int. J. Multiphase Flow 25 (6–7) (1999) 1073–1097.
[30] Shaik, Versteeg, Model for the prediction of internal flow conditions in pressurised metered dose inhalers (pMDIs), Drug Deliv. Lung 19 (2008) 10–12.
[31] P. Sheth, S.W. Stein, P.B. Myrdal, Factors influencing aerodynamic particle size distribution of suspension pressurized metered dose inhalers, AAPS PharmSciTech 16 (1) (2014) 192–201.
[32] H. Smyth, A.J. Hickey, G. Brace, T. Barbour, J. Gallion, J. Grove, Spray pattern analysis for metered dose inhalers I: orifice size, particle size, and droplet motion correlations, Drug Dev. Ind. Pharm. 32 (9) (2006) 1033–1041.
[33] H. Smyth, The influence of formulation variables on the performance of alternative propellant-driven metered dose inhalers, Adv. Drug Deliv. Rev. 55 (7) (2003) 807–828.
[34] S.W. Stein, P. Sheth, P.B. Myrdal, A model for predicting size distributions delivered from pMDIs with suspended drug, Int. J. Pharm. 422 (1–2) (2012) 101–115.
[35] S.W. Stein, P. Sheth, P.D. Hodson, P.B. Myrdal, Advances in metered dose inhaler technology: hardware development, AAPS PharmSciTech 15 (2) (2014) 326–338.
[36] C. Terzano, Pressurized metered dose inhalers and add-on devices, Pulm. Pharmacol. Ther. 14 (5) (2001) 351–366.
[37] H.K. Versteeg, G.K. Hargrave, M. Kirby, Internal flow and near-orifice spray visualisations of a model pharmaceutical pressurised metered dose inhaler, Journal of Physics: Conference Series, vol. 45, IOP Publishing 2006, p. 028, No. 1.
[38] G.B. Wallis, One-Dimensional Two-Phase Flow, McGraw-Hill, 1969.
[39] C.S. Kim, D. Trujillo, M.A. Sackner, Size aspects of metered-dose inhaler aerosols, American Review of Respiratory Disease 132 (1) (1985) 137–142.